*molecules*

*Article*

# Surface Properties and Photocatalytic Activity of KTaO₃, CdS, MoS₂ Semiconductors and Their Binary and Ternary Semiconductor Composites

**Beata Bajorowicz [1], Anna Cybula [1], Michał J. Winiarski [2], Tomasz Klimczuk [2] and Adriana Zaleska [1,\*]**

[1]  Department of Chemical Technology, Faculty of Chemistry, Gdansk University of Technology, ul. G. Narutowicza 11/12, Gdansk 80-233, Poland; E-Mails: beatabajorowicz@gmail.com (B.B.); anna-cybula@wp.pl (A.C.)

[2]  Department of Solid State Physics, Faculty of Applied Physics and Mathematics, Gdansk University of Technology, ul. G. Narutowicza 11/12, Gdansk 80-233, Poland; E-Mails: mwiniarski@mif.pg.gda.pl (M.J.W.); tomasz.klimczuk@pg.gda.pl (T.K.)

**\***  Author to whom correspondence should be addressed; E-Mail: adriana.zaleska@pg.gda.pl; Tel.: +48-58-347-24-37; Fax: +48-58-347-20-65.

**Abstract:** Single semiconductors such as KTaO₃, CdS MoS₂ or their precursor solutions were combined to form novel binary and ternary semiconductor nanocomposites by the calcination or by the hydro/solvothermal mixed solutions methods, respectively. The aim of this work was to study the influence of preparation method as well as type and amount of the composite components on the surface properties and photocatalytic activity of the new semiconducting photoactive materials. We presented different binary and ternary combinations of the above semiconductors for phenol and toluene photocatalytic degradation and characterized by X-ray powder diffraction (XRD), UV-Vis diffuse reflectance spectroscopy (DRS), scanning electron microscopy (SEM), Brunauer–Emmett–Teller (BET) specific surface area and porosity. The results showed that loading MoS₂ onto CdS as well as loading CdS onto KTaO₃ significantly enhanced absorption properties as compared with single semiconductors. The highest photocatalytic activity in phenol degradation reaction under both UV-Vis and visible light irradiation and very good stability in toluene removal was observed for ternary hybrid obtained by calcination of KTaO₃, CdS, MoS₂ powders at the 10:5:1 molar ratio. Enhanced photoactivity could be

related to the two-photon excitation in KTaO$_3$-CdS-MoS$_2$ composite under UV-Vis and/or to additional presence of CdMoO$_4$ working as co-catalyst.

## 1. Introduction

Since the discovery of the photocatalytic splitting of water on TiO$_2$ photochemical electrodes by Fujishima and Honda in 1972 [1], semiconductor-based photocatalysts have attracted increasing interest due to their potential applications in solar energy conversion, hydrogen evolution and photodegradation of organic pollutants [2–11]. Among different photocatalysts, titanium dioxide has become the most studied and widely used semiconductor material, however, it can only be excited by UV light, leading to low efficiency for utilizing solar energy [12]. Therefore, it is still of great importance to develop new types of photocatalysts which should be highly active, photostable and activated by low powered and low cost irradiation sources. Furthermore, one of the promising approaches is combining some semiconductors to form composites which can improve the efficiency of a photocatalytic system because of novel or enhanced properties that do not exist in individual components [13–16]. It was demonstrated that the Bi$_2$WO$_6$-based photocatalysts systems could be efficiently used in chemical synthesis and fuel production [7], whilst the graphene based composites seem to be a promising material for solar energy conversion and selective transformations of organic compounds [11]. Zhang *et al.* showed that the nanocomposites of TiO$_2$-graphene exhibits much higher photocatalytic activity and stability than bare titanium dioxide toward the gas-phase degradation of benzene [17].

Among semiconductors, potassium tantalate with a wide band gap could be an interesting alternative to the well-known titanium dioxide. Tantalates possess conduction bands consisting of Ta5d orbitals located at a more negative position than titanates (Ti3d) or niobates (Nb4d). Therefore, the high potential of the conduction band of tantalates could lead to being more advantageous in the photocatalytic reaction [18]. It has been reported by Liu *et al.* that sodium and potassium tantalates showed higher activities for water splitting than those of niobates synthesized by hydrothermal route. Moreover, the highest photocatalytic activity was exhibited by NaTaO$_3$ powder with cubic crystalline structure [19]. It was also observed that when NiO co-catalysts were loaded on the tantalate semiconductors, the photocatalytic activities were drastically increased [20]. Furthermore, there could be correlation between the photocatalytic activity of ABO$_3$ tantalates and preparation method as well as their crystal structure. Lin *et al.* showed that sol gel sodium tantalate with monoclinic crystalline structures exhibited higher photoactivity for water splitting than that with orthorhombic structure and obtained by solid-state method [21]. In other study Torres-Martínez *et al.* prepared sodium tantalate samples doped with Sm and La using sol-gel or solid state reaction methods. The best half-life time ($t_{1/2} = 65$ min) of photocatalytic degradation of methylene blue under UV light was shown by NaTaO$_3$ doped with Sm obtained by sol-gel technique and heat treated at 600 °C [22]. However, in the literature there is still not enough information about photocatalytic activity of tantalate for degradation of organic pollutants, especially potassium tantalate has received very little research attention in this area.

In contrast to potassium tantalate, cadmium sulfide is among the most exhaustively investigated semiconductors. It has a wide range of applications, including solar cells, optoelectronic devices, fluorescence probes, sensors, laser light-emitting diodes and photocatalysis [23–25]. Unfortunately, bare CdS photocatalyst has very low separation efficiency of photogenerated electron-hole pairs and undergoes photocorrosion which limit its practical application [26]. In order to improve photoactivity and to inhibit the photocorrosion, cadmium sulfide is usually coupled with other semiconductors, including $CdS/TiO_2$ [27–29], CdS/ZnO [30,31], CdS/ZnS [32], $CdS/WO_3$ [33] as well as $CdS/MoS_2$. In particular, $MoS_2$ semiconductor is an efficient co-catalyst. Moreover, the unique layered structure of $MoS_2$ endows many important properties, such as anisotropy, chemical stability and anti-photo corrosion. [34]. There were few studies on the $MoS_2$-CdS system obtained by impregnation [35], ball-milling combined calcination [36], electrodeposition and chemical bath deposition [37] or hydrothermal [38] methods for hydrogen production under visible light. Zong *et al.* showed that individual CdS and $MoS_2$ particles were almost inactive in hydrogen evolution compared to the $MoS_2$ particles deposited onto CdS. Moreover, researchers observed that the rate of hydrogen evolution on $MoS_2$/CdS was higher than on CdS particles loaded with other catalysts such as Pt, Ru, Rh, Pd and Au. This result was explained by the better electron transfer between $MoS_2$ and CdS [39].

Binary and ternary composites based on potassium tantalate, cadmium sulfide and molybdenum disulfide could be new examples of photoactive materials. In this study we obtained various combinations of $KTaO_3$, CdS, $MoS_2$ single semiconductors as well as their precursor solutions using calcination and hydro/solvothermal routes. The effect of the preparation method, type and amount of the composite components on the surface properties and photocatalytic activity in phenol degradation in the aqueous phase as well as activity and photostability in toluene degradation in the gas phase was investigated. Light emitting diodes (LEDs) were used in the gas phase measurements as a promising irradiation source, which allow to reduce power consumption and costs of photocatalytic processes.

## 2. Results and Discussion

### 2.1. BET Surface Area

The surface area and the pore volume of $KTaO_3$, CdS, $MoS_2$ semiconductors and their binary and ternary composites prepared by hydro/solvothermal as well as hydro/solvothermal mixed solutions and calcination methods are summarized in Table 1. The surface area of as-prepared samples fluctuated from less than 0.1 to 17.5 $m^2$/g and was dependent on type and amounts of semiconductors as well as preparation methods. The pure CdS and $MoS_2$ semiconductors had BET surface area about 1.2 and 1.8 $m^2$/g, respectively. The CdS-$MoS_2$ composites containing more or the same amounts of CdS as $MoS_2$ caused an increase in surface area whereas in the presence of the excess $MoS_2$ in the composite a drop in the surface area was observed as compared with pure semiconductors. The sample CdS-$MoS_2$ 4-1 presented the highest surface area (about 11.1 $m^2$/g) from among CdS-$MoS_2$ composites. The $KTaO_3$-based composites prepared by hydro/solvothermal methods had higher BET surface areas than composites which were calcined. Extremely small surface area and nearly zero pore volume were observed for the $KTaO_3$-$MoS_2$ 10-1_C and $KTaO_3$-CdS-$MoS_2$ 10-1-1_C samples. In the case of binary $KTaO_3$-based composites it could be seen that potassium tantalate containing a small amount of $MoS_2$

had lower surface area than potassium tantalate containing a small amount of CdS. Moreover, in the case of ternary composites it could be also observed that the high loading of CdS resulted in a significant increase in surface area. The pore volumes of obtained photocatalysts were very low and fluctuated from zero to 0.0088 $cm^3$/g. It was observed that the pore volumes increased with increasing the surface area.

**Table 1.** Sample label, preparation method, BET surface area and pore volume of obtained single semiconductors and their composites.

| Sample Label | $KTaO_3$:CdS:$MoS_2$/ Molar Ratio | Preparation Method | BET Surface Area/ [$m^2$/g] | Pore Volume/ [$cm^3$/g] |
|---|---|---|---|---|
| $KTaO_3$ | 1:0:0 | hydrothermal | 0.1 | 0.0001 |
| CdS | 0:1:0 | solvothermal | 1.2 | 0.0006 |
| $MoS_2$ | 0:0:1 | hydrothermal | 1.8 | 0.0009 |
| CdS-$MoS_2$ 5-1 | 0:5:1 | solvothermal mixed solutions | 5.0 | 0.0026 |
| CdS-$MoS_2$ 4-1 | 0:4:1 | solvothermal mixed solutions | 11.1 | 0.0056 |
| CdS-$MoS_2$ 1-1 | 0:1:1 | solvothermal mixed solutions | 10.4 | 0.0052 |
| CdS-$MoS_2$ 1-5 | 0:1:5 | solvothermal mixed solutions | 1.0 | 0.0006 |
| $KTaO_3$-CdS 10-1_MS | 10:1:0 | solvothermal mixed solutions | 17.5 | 0.0088 |
| $KTaO_3$-CdS 10-1_C | 10:1:0 | hydro/solvothermal and calcination | 0.4 | 0.0002 |
| $KTaO_3$-$MoS_2$ 10-1_MS | 10:0:1 | hydrothermal mixed solutions | 2.8 | 0.0014 |
| $KTaO_3$-$MoS_2$ 10-1_C | 10:0:1 | hydrothermal and calcination | <0.1 | ~0 |
| $KTaO_3$-CdS-$MoS_2$ 10-1-1_MS | 10:1:1 | solvothermal mixed solutions | 4.0 | 0.0019 |
| $KTaO_3$-CdS-$MoS_2$ 10-1-1_C | 10:1:1 | hydro/solvothermal and calcination | <0.1 | ~0 |
| $KTaO_3$-CdS-$MoS_2$ 10-5-1_MS | 10:5:1 | solvothermal mixed solutions | 10.3 | 0.0051 |
| $KTaO_3$-CdS-$MoS_2$ 10-5-1_C | 10:5:1 | hydro/solvothermal and calcination | 0.5 | 0.0003 |

## *2.2. XRD Analysis*

Figure 1a shows XRD patterns for pure CdS and $MoS_2$ as well as CdS-$MoS_2$ samples with different CdS:$MoS_2$ molar ratio. Low observed intensity of the XRD peaks for $MoS_2$ and for CdS-$MoS_2$ with 1:5 ratio is likely caused by low crystallinity of the $MoS_2$ compound. As can be seen, adding less than 20% of CdS to $MoS_2$ causes a dramatic change in XRD pattern. CdS is a dominant phase and $MoS_2$ is hardly present. No traces of $MoS_2$ have been found for higher CdS concentration (CdS-$MoS_2$ 1:1 and CdS-$MoS_2$ 5:1 samples). Lattice parameters for CdS (*P6_3mc*, s.g. #186) were refined by using the LeBail method.

For CdS we obtained a = 4.1341(8) Å and c = 6.710(1) Å in very good agreement with reported by Wiedemeire *et al.* [40]. Adding $MoS_2$ does not change *a* lattice parameter, whereas *c* increases with increasing $MoS_2$ and for the sample which contains the highest amount of $MoS_2$ (sample b) the refined *c* is 6.733(3) Å. This clear change of the unit cell size and relative change of the intensity of three most dominant XRD peaks between 24 and 29 degrees, allow us to conclude that Mo atoms are incorporated into CdS hexagonal crystal structure. Figure 1b displays powder X-ray diffraction patterns for pure $KTaO_3$ prepared by the hydrothermal method. Two different methods were used to obtain $KTaO_3$-CdS and $KTaO_3$-$MoS_2$ composites. As can be seen from the XRD patterns for $KTaO_3$-CdS 10:1_C and $KTaO_3$-$MoS_2$ 10:1_C samples, the calcination method does not produce new phases and $KTaO_3$

together with CdS are observed. For the latest compound the most intense peaks are hardly visible between 25 and 30 deg. Contrary to the calcination method, the hydro/solvothermal mixed solutions route produces more complex compounds. For the system with CdS, the majority phase is $Ta_2O_5$ with small amount of $TaS_2$ and $K_2Ta_{15}O_{32}$. For the system with $MoS_2$ almost pure pyrochlore-like $K_2Ta_2O_6$ was found. This defect pyrochlore structure was described in details and also tested as a photocatalyst by Hu *et al.* [41].

**Figure 1.** Powder XRD patterns for (**a**) single CdS, $MoS_2$ and binary CdS-$MoS_2$ nanocomposites, (**b**) single $KTaO_3$ and binary $KTaO_3$-based nanocomposites, (**c**) ternary $KTaO_3$-based nanocomposites.
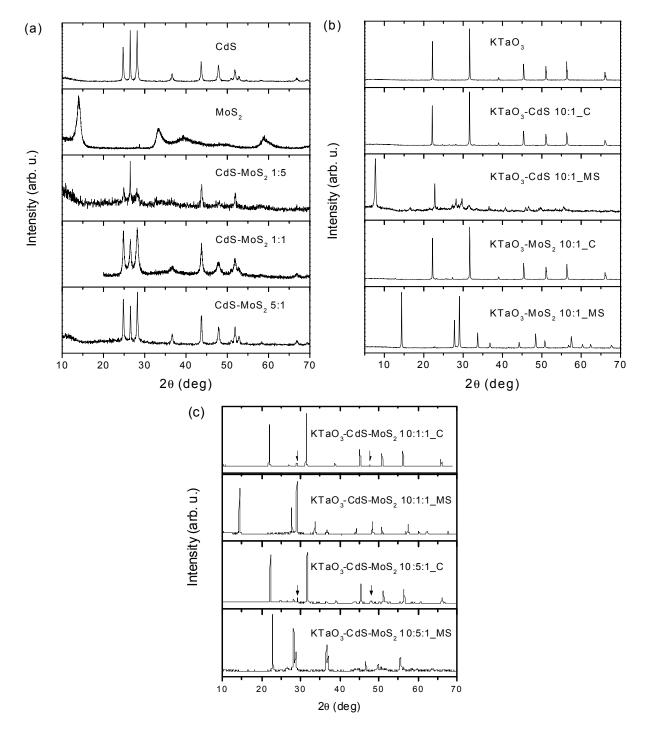
Figure 1c shows XRD patterns for ternary $KTaO_3$-CdS-$MoS_2$ composites with two different molar ratios and two various preparation routes. Similarly to what was observed for binary composites produced by calcination method, the majority phase is $KTaO_3$, however, a small amount of $CdMoO_4$ emerges with the two most intense peaks marked by arrow. While the solvothermal mixed solutions method causes decomposition of $KTaO_3$, the main products detected are $K_2Ta_2O_6$ and $Ta_2O_5$ together with Mo-doped CdS for the sample 10:1:1 and 10:5:1, respectively.

*2.3. Morphology*

The morphology of the products was observed by SEM and is presented in the Figures 2–5. Figure 2 shows an SEM image of single semiconductors prepared by hydro/solvothermal methods. As clearly shown, the $KTaO_3$ have a cube-like shape with various sizes. Using higher magnification image of these particles, we notice that small $KTaO_3$ nanocubes with an average size of about 0.2–1 μm grow at the surface of bigger cubes having widths of 5–8 μm. Pure CdS clearly indicates nanoleaf structures having the length of about 3 μm. In the case of $MoS_2$ we observed that the product has the shape of flower-like microspheres with an average diameter of 5 μm.

**Figure 2.** SEM images of single semiconductors obtained by hydrothermal method: (**a**,**b**) $KTaO_3$; (**c**) CdS; (**d**) $MoS_2$.
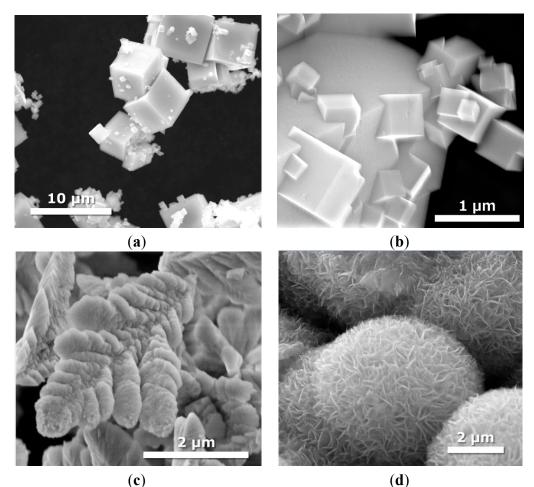
Figure 3 shows SEM images of binary CdS-MoS$_2$ composites with different CdS and MoS$_2$ molar ratios. In the case of CdS-MoS$_2$ 5-1 sample containing the highest molar ratio of CdS, we still observed nanoleaf structure indicating the presence of CdS. XRD analysis also showed that no traces of MoS$_2$ have been found for higher CdS concentration. The increase of MoS$_2$ ratio resulted in the formation of hexagonal shaped nanostructures with average edge size of about 100–125 nm (Figure 3b).

As can be seen from Figure 3c,d, further increase in molar ratio of MoS$_2$ to CdS causes a large change in microstructures. We can observe bonded structures of microspheres with diameters ranging from 0.08 to 1 μm.

**Figure 3.** SEM images of binary CdS-MoS$_2$ composites obtained by solvothermal mixed solution methods with different molar ratio of CdS: (**a**) CdS:MoS$_2$ = 5:1; (sample CdS-MoS$_2$ 5-1); (**b**) CdS:MoS$_2$ = 4:1 (sample CdS-MoS$_2$ 4-1); (**c**) CdS:MoS$_2$ = 1:1 (sample CdS-MoS$_2$ 1-1); and (**d**) CdS:MoS$_2$ = 1:5 (sample CdS-MoS$_2$ 1-5).



(**a**)                                                                                  (**b**)

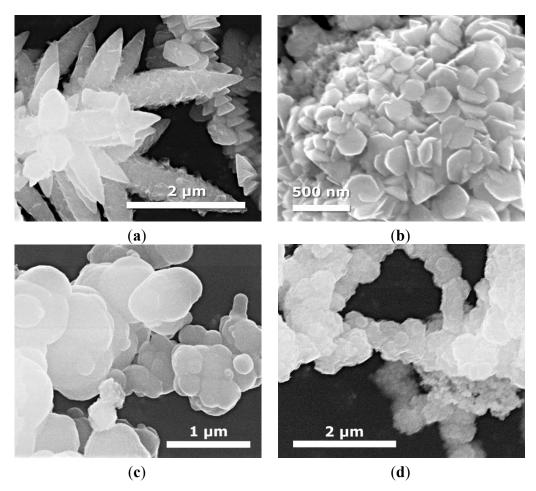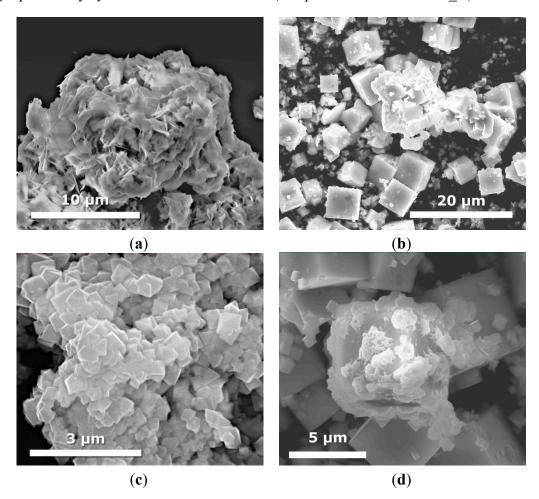(**c**)                                                                                  (**d**)

Figure 4 displays SEM images of binary KTaO$_3$-CdS and KTaO$_3$-MoS$_2$ composites prepared by two different routes. In the case of the KTaO$_3$-CdS and KTaO$_3$-MoS$_2$ samples, which were obtained by calcination, we can see mainly the structure of cubes, which indicates the presence of KTaO$_3$. In contrast, the solvothermal mixed solutions route leads to the formation of other nanostructures, suggesting the presence of more complex compounds: K$_2$Ta$_{15}$O$_{32}$, Ta$_2$O$_5$, TaS$_2$ and K$_2$Ta$_2$O$_6$ for the system with CdS and MoS$_2$ which were confirmed by XRD analysis. The transition of the KTaO$_3$ structure from cubic to octahedral was observed for the samples KTaO$_3$-MoS$_2$ 10-1 and KTaO$_3$-CdS-MoS$_2$ 10-1-1 obtained by

solvothermal mixed solutions. In the case of calcinated $KTaO_3$-CdS-$MoS_2$ 10-5-1 composite we can see nanoleaves of CdS deposited on the surface of large cubes of $KTaO_3$ (Figure 5d). Contrary to calcination, solvothermal mixed solutions method causes dramatic changes in the structure—neither cubes nor nanoleaf are observed (Figure 5c).

**Figure 4.** SEM images of binary $KTaO_3$-CdS and $KTaO_3$-$MoS_2$ composites obtained with different molar ratio and using two preparation routes: (**a**) $KTaO_3$-CdS (10:1) obtained by solvothermal mixed solutions (sample $KTaO_3$-CdS 10-1_MS); (**b**) $KTaO_3$-CdS (10:1) obtained by calcination of single previously synthesized semiconductors (sample $KTaO_3$-CdS 10-1_C); (**c**) $KTaO_3$-$MoS_2$ (10:1) obtained by solvothermal mixed solutions (sample $KTaO_3$-$MoS_2$ 10-1_MS); and (**d**) $KTaO_3$-$MoS_2$ (10:1) obtained by calcination of single previously synthesized semiconductors (sample $KTaO_3$-$MoS_2$ 10-1_C).



(**a**)
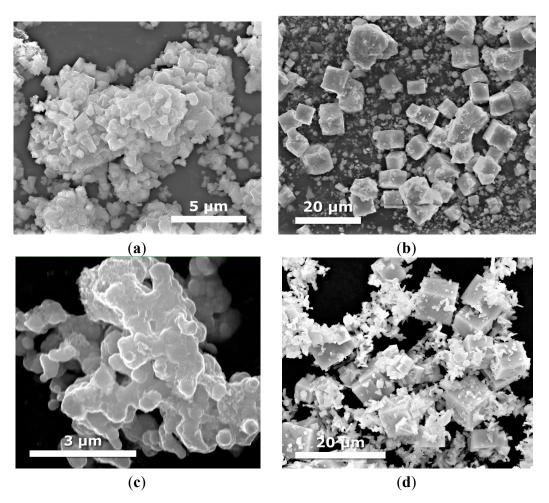
(**b**)

(**c**)

(**d**)

## 2.4. UV-Vis Properties

DRS UV-Vis absorption spectra in the wavelength range of 200–800 nm of as-prepared samples were investigated and the results are shown in Figure 6a–c. Figure 6a depicts the spectra for pure CdS and $MoS_2$ semiconductors and their binary composites with varying molar ratio between CdS and $MoS_2$. As it can be seen, all the samples could absorb both UV and visible light. The absorption edge of single CdS is at about 510 nm, which coincides with the literature. Moreover, it was previously reported that the absorption properties of CdS are strongly shape-dependent [42]. It could also be seen

that the loading of MoS$_2$ on CdS improved the light absorption as compared with pure CdS. Liu *et al.* also presented enhanced absorption properties for CdS-MoS$_2$ composites to photocatalytic H$_2$ production [38]. In comparison with single CdS, composites with excess of CdS exhibited a red-shift and a less steep absorption edge.
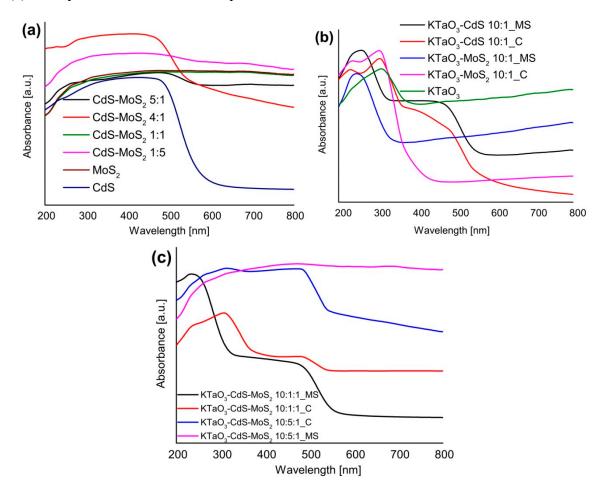
**Figure 5.** SEM images of ternary KTaO$_3$-CdS-MoS$_2$ composites obtained with different molar ratio and using two different preparation route: (**a**) KTaO$_3$-CdS-MoS$_2$ (10:1:1) obtained by solvothermal mixed solutions (sample KTaO$_3$-CdS-MoS$_2$ 10-1-1_MS); (**b**) KTaO$_3$-CdS-MoS$_2$ (10:1:1) obtained by calcination of single previously synthesized semiconductors (sample KTaO$_3$-CdS-MoS$_2$ 10-1-1_C); (**c**) KTaO$_3$-CdS-MoS$_2$ (10:5:1) obtained by solvothermal mixed solutions (sample KTaO$_3$-CdS-MoS$_2$ 10-5-1_MS); and (**d**) KTaO$_3$-CdS-MoS$_2$ (10:5:1) obtained by calcination of single previously synthesized semiconductors (sample KTaO$_3$-CdS-MoS$_2$ 10-5-1_C).

(**a**)

(**b**)

(**c**)

(**d**)

The absorbance was very similar for pure MoS$_2$ and composite with 1:1 molar ratio between components. However, for composites containing excess MoS$_2$, absorption was more intense. Figure 6b displays absorption spectra of single KTaO$_3$ and binary KTaO$_3$-based composites containing small amounts of CdS or MoS$_2$ and prepared by two different procedures. In the case of single KTaO$_3$, there is an obvious absorption band centered at about 310 nm and no absorption peak is detected above 310 nm. For octahedral KTaO$_3$ nanocrystalline obtained by Zou *et al.* using hydrothermal method, the absorption peak was detected at 265 nm [43]. It was also observed that binary KTaO$_3$-based composites

loaded with small amount of CdS or MoS2 had steeper absorption edges and maximum absorption shifted to shorter wavelengths as compared with single potassium tantalate. Moreover, KTaO3-CdS composites showed second steep absorption edges in the visible light region. Figure 6c shows the spectra for ternary KTaO3-CdS-MoS2 composites containing different amount of CdS and prepared by various methods. Loading of larger amounts of CdS onto KTaO3-CdS-MoS2 composites significantly improved the spectral absorption. For ternary composites containing greater amount of cadmium sulfide and obtained by both methods, there were widest absorption ranges among all obtained samples but only for a calcined composite a steep absorption edge (at about 510 nm) was observed. In general, loading MoS2 onto CdS shifted absorbance peaks to longer wavelengths, just as loading CdS onto KTaO3 enhanced absorption features. It may be suggested that the best adsorption properties could probably be achieved for the ternary KTaO3-CdS-MoS2 composites containing appropriate molar ratio between semiconductors.

**Figure 6.** The UV-Vis diffuse reflectance spectra of (**a**) single CdS, MoS2, and binary CdS-MoS2 nanocomposites, (**b**) single KTaO3 and binary KTaO3-based nanocomposites, (**c**) ternary KTaO3-based nanocomposites.



## 2.5. The Photocatalytic Degradation of Phenol in the Aqueous Phase

Photocatalytic activity of as-prepared semiconductors and their nanocomposites was estimated by examining the reaction of phenol degradation in the presence of UV-Vis light irradiation and for

selected samples photoactivity under visible light was also analyzed. No degradation of phenol was observed in the absence of photocatalyst or illumination. Photocatalytic activity under UV-Vis and visible light is presented as phenol degradation rate (Table 2) and as efficiency of phenol removal after 60 min of irradiation (Figures 7 and 8). Commercially available P25 TiO$_2$ was used as a standard reference material in photocatalytic activity measurements.

**Figure 7.** The percentage degradation of phenol at various time intervals under UV-Vis light in the presence: (**a**) single CdS, MoS$_2$, and CdS-MoS$_2$ nanocomposites; (**b**) single KTaO$_3$ and binary KTaO$_3$-based nanocomposites; (**c**) ternary KTaO$_3$-based nanocomposites.
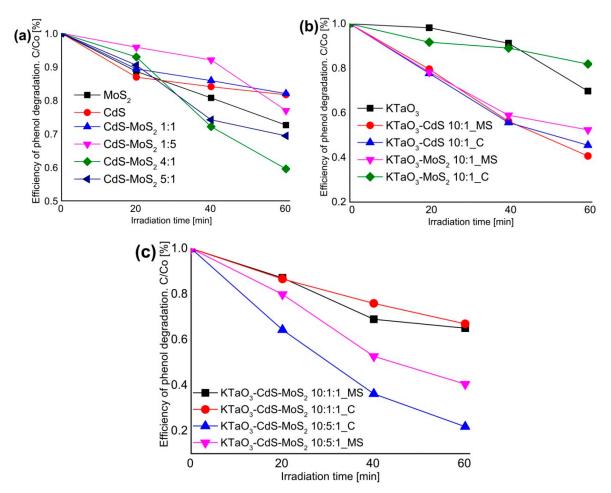


Figure 7a shows the results of phenol degradation under UV-Vis light in the presence of pure CdS and MoS$_2$, and their binary composites synthesized by hydro/solvothermal methods. In comparison with pure CdS and MoS$_2$, photocatalytic activity for degradation of phenol increased in the presence of CdS-MoS$_2$ nanocomposites containing excess of CdS. In the presence of CdS-MoS$_2$ 4:1 and CdS-MoS$_2$ 5:1, the percentage degradation of phenol after 60 min was about 41% and 31%, respectively, which indicates that with decreasing excess of CdS, the photocatalytic activity is relatively higher. For composites containing more or the same amount of MoS$_2$ as CdS, photoactivity was comparable with pure semiconductors. The highest phenol degradation rate, about 1.41 $\mu$mol·dm$^{-3}$·min$^{-1}$, was observed in the case of the CdS-MoS$_2$ 4:1 composite. For the other samples degradation rates were low and fluctuated from 0.62 to 0.90 $\mu$mol·dm$^{-3}$·min$^{-1}$. Zong and co-workers reported that the photocatalytic H$_2$ production achieved a maximum when the loading amount of MoS$_2$ on CdS was about 0.2 wt % [39].

Figure 7b displays the results of phenol degradation under UV-Vis light in the presence of single $KTaO_3$ and binary potassium tantalate-based composites containing a small amount of CdS or $MoS_2$ and prepared by different routes. The phenol degradation after 60 min of irradiation was only 18% in the case of the calcined $KTaO_3$-$MoS_2$ sample, which is lower than in the presence of single $KTaO_3$ (about 30%). While for the $KTaO_3$-$MoS_2$ sample obtained by hydrothermal method phenol degradation was more efficient (about 48%). It could be also observed that photoactivities were similar and increased to 59% and 55% for $KTaO_3$-CdS 10-1 composites prepared by hydrothermal and calcination method, respectively. It may be suggested that loading cadmium sulfide onto $KTaO_3$ enhanced photoactivity, while the influence of introduction of molybdenum disulfide on the photoactivity was dependent on preparation technique. Figure 7c depicts the results of phenol degradation under UV-Vis light for ternary $KTaO_3$-CdS-$MoS_2$ composites containing various amounts of CdS as well as prepared by different methods. In general, more addition of CdS significantly enhanced the photocatalytic activity of ternary composites. In the presence of the $KTaO_3$-CdS-$MoS_2$ 10-1-1 sample the percentage degradation of phenol was low (about 35%) and quite comparable for both methods. In the case of the $KTaO_3$-CdS-$MoS_2$ 10-5-1 composites photoactivities were much more efficient. After 60 min of irradiation, for the sample prepared by hydro/solvothermal method phenol degradation reached 60%. At the same time in the presence of the $KTaO_3$-CdS-$MoS_2$ 10-5-1 sample prepared by the calcination method about 80% of phenol was degraded and it was the highest efficiency among all obtained samples. Therefore, appropriate ratio between $KTaO_3$, CdS and $MoS_2$ semiconductors in the composites is supposed to be responsible for the highest efficiency of phenol photodegradation. This deduction coincides with the UV-Vis properties of obtained samples described in Section 3.3.

**Figure 8.** The percentage degradation of phenol at various time intervals under visible light in the presence of selected composites.
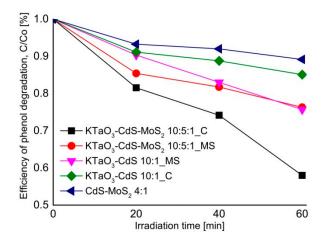


Figure 8 shows the results of phenol degradation under visible light for selected samples which exhibited the highest efficiency of phenol degradation under UV-Vis light irradiation. Among these, the highest activity (about 42%) after 60 min of visible irradiation was also exhibited by calcined ternary $KTaO_3$-CdS-$MoS_2$ 10-5-1 composites. In the case of the binary calcined composite containing small amount of CdS, photoactivity reached about 15%. In the presence of samples obtained by the solvothermal mixed solutions route activity was more efficient (24%). The lowest activity (about 11%) was observed for the composite containing CdS and $MoS_2$ at the 4:1 molar ratio.

## 2.6. The Photocatalytic Degradation of Toluene in the Gas Phase

The photocatalytic activity and stability of as-prepared photocatalysts were also evaluated by degradation of the toluene in the gas phase under UV light irradiation using low powered irradiation source, e.g., LEDs ($\lambda_{max}$ = 375 nm) in four subsequent measurement cycles. The efficiency of toluene photodegradation after 60 min in the presence of as-prepared semiconductor samples is given in Table 2.

It could be seen that CdS, KTaO$_3$ and MoS$_2$ semiconductors and their composites were photoactive in toluene degradation. In the case of single semiconductors, removal efficiency in the presence of CdS reached about 57% after a 60-min process and activity was stable in four subsequent cycles of irradiation. While in the presence of KTaO$_3$ and MoS$_2$ photocatalytic activity decreased from 64% and 46% (1st cycle) to 37% and 22% (4th cycle), respectively. The highest activity and stability under UV light irradiation from all among CdS-MoS$_2$ composites was exhibited by samples at the molar ratio 4:1 and 1:1.

**Table 2.** Photocatalytic activities of obtained samples for toluene photodegradation in four subsequent measurement cycles and for phenol degradation presented as phenol degradation rate.

| Sample Label | Phenol Degradation Rate under UV-Vis/($\mu$mol·dm$^{-3}$·min$^{-1}$) | Toluene Degradation after 1 h Irradiation (LEDs, $\lambda_{max}$ = 375 nm) [%] | | | |
|---|---|---|---|---|---|
| | | 1st Cycle | 2nd Cycle | 3rd Cycle | 4th Cycle |
| KTaO$_3$ | 0.79 | 64 | 63 | 42 | 37 |
| CdS | 0.61 | 57 | 57 | 57 | 52 |
| MoS$_2$ | 0.90 | 46 | 23 | 22 | 22 |
| CdS-MoS$_2$ 1-5 | 0.77 | 57 | 53 | 44 | 27 |
| CdS-MoS$_2$ 1-1 | 0.62 | 61 | 53 | 62 | 52 |
| CdS-MoS$_2$ 5-1 | 0.81 | 70 | 60 | 49 | 48 |
| CdS-MoS$_2$ 4-1 | 1.41 | 53 | 56 | 60 | 62 |
| KTaO$_3$-CdS 10-1_MS | 2.08 | 47 | 45 | 41 | 40 |
| KTaO$_3$-CdS 10-1_C | 1.75 | 53 | 48 | 52 | 50 |
| KTaO$_3$-MoS$_2$ 10-1_MS | 1.69 | 55 | 51 | 49 | 51 |
| KTaO$_3$-MoS$_2$ 10-1_C | 0.55 | 46 | 34 | 37 | 35 |
| KTaO$_3$-CdS-MoS$_2$ 10-1-1_MS | 1.15 | 50 | 52 | 48 | 39 |
| KTaO$_3$-CdS-MoS$_2$ 10-1-1_C | 1.11 | 53 | 54 | 49 | 40 |
| KTaO$_3$-CdS-MoS$_2$ 10-5-1_MS | 1.99 | 50 | 41 | 43 | 41 |
| KTaO$_3$-CdS-MoS$_2$ 10-5-1_C | 2.81 | 48 | 48 | 50 | 46 |
| TiO$_2$ (P25) | 2.87 | 98 | 96 | 95 | 95 |

The lowest photostability presented the CdS-MoS$_2$ sample when the molar ratio was 1:5. It suggests that an excess of MoS$_2$ caused the decrease in photostability. The CdS-MoS$_2$ composite at the molar ratio 5:1 exhibited the highest activity in the 1st cycle (about 70%) but this activity decreased to 48% in the 4th cycle of photoirradiation. In the case of binary KTaO$_3$-based composites it was observed that the photoactivity about 50% and the best stability during four cycles of irradiation was exhibited by potassium tantalate with a small amount of cadmium sulfide (KTaO$_3$-CdS 10-1 sample) prepared by the calcination method and potassium tantalate with molybdenum disulfide (KTaO$_3$-MoS$_2$ 10-1

sample) obtained by the hydrothermal mixed solutions route. While the photocatalytic activity of the KTaO$_3$-MoS$_2$ 10-1 sample prepared by calcination method after four cycles of irradiation was less by 11% as compared with the first cycle. It indicates that the activity is dependent not only on the type and content of the composite components but also on the preparation method. All of prepared ternary KTaO$_3$-CdS-MoS$_2$ composites exhibited about 50% efficiency degradation of toluene after the 1st cycle of irradiation, but activity didn't change after four cycles only in the case of the sample KTaO$_3$-CdS-MoS$_2$ 10-5-1 obtained by the calcination method.

## 2.7. The Origin of Photocatalytic Activity

UV and visible light induced photoactivity presented as efficiency of phenol removal after 60-min irradiation for the most active binary and ternary composites is shown in Figure 9. Highest activity under UV-Vis light of KTaO$_3$-CdS-MoS$_2$ (10:5:1) composite, obtained by solvothermal preparation of single semiconductors followed by calcination, could be related to the presence of heterojunctions between semiconductors. One pot reaction used for preparation of the KTaO$_3$-CdS-MoS$_2$ composite did not allow the formation of well-developed crystal structure of all semiconductors, as was shown in XRD analysis. However, the structure obtained by the sintering of three components could favors photogenerated charge carriers transfer between phase boundary of semiconductors resulted in higher photoactivity. The KTaO$_3$-CdS-MoS$_2$ nanocomposite could be excited by two photons due to utilization of a heterojunction between KTaO$_3$ with two low band gap semiconductors (*i.e.*, CdS and MoS$_2$). As shown in Figure 10, UV light could induce excitation in solid KTaO$_3$ ($E_g$ = 3.4 eV) and generate free electrons ($e^-$) and holes ($h^+$). Since the VB position of KTaO$_3$ (+3.1 V) is lower than the VB band of MoS$_2$ (+1.8 V), $h^+$ transfer would then occur from KTaO$_3$ to MoS$_2$. At the same time UV or visible light could be absorbed by CdS ($E_g$ = 2.5 eV) and generate $e^-$ and $h^+$ in CdS. As the CB position of CdS (−0.6 V) is higher in energy than the CB of solid MoS$_2$ (+0.05 V), electron transfer could occur from CdS to MoS$_2$, thereby causing charge separation at the CdS-MoS$_2$ junction. Finally positioning the CB of KTaO$_3$ (−0.3 V) higher in energy than the VB of CdS (+1.8 V) causes $e^-$ transfer from KTaO$_3$ to CdS and recombination of $e^-$ in KTaO$_3$ with $h^+$ generated in CdS, thus completing the photoexcitation cycle in which the excited state of MoS$_2$ has been achieved via a two-photon process. Thus, organic compounds (such as phenol or toluene) could be degraded via active oxygen species generated at the surface of excited MoS$_2$ in two photons process.

Additionally, higher activity under UV-Vis light of the KTaO$_3$-CdS-MoS$_2$ 10-5-1_C sample could be also related to the presence of CdMoO$_4$ detected by XRD analysis (see Figure 1c). Photocatalytic activity of pure and *Ag*-modified CdMoO$_4$ under simulate solar irradiation was reported by others [44,45]. The valence band of CdMoO$_4$ consists of the hybrid orbitals of O 2p as well as Cd 6s and the conduction band consists of Mo 4d orbital and the band gap energies between them is about 3.4 eV. Thus, CdMoO$_4$ presented at the surface of composite could also adsorb UV light and enhance activity in observed photodegradation reaction. Lower UV and Vis-induced photoactivity of KTaO$_3$-CdS-MoS$_2$ (10:5:1) composite obtained by mixed solvothermal reaction, comparing to that one prepared by calcination step, could be related the decomposition of KTaO$_3$ and formation of K$_2$Ta$_2$O$_6$ and Ta$_2$O$_5$ as main component of as-prepared samples.

**Figure 9.** Efficiency of phenol removal under UV-Vis and visible light (λ > 420 nm) for selected binary and ternary composites.
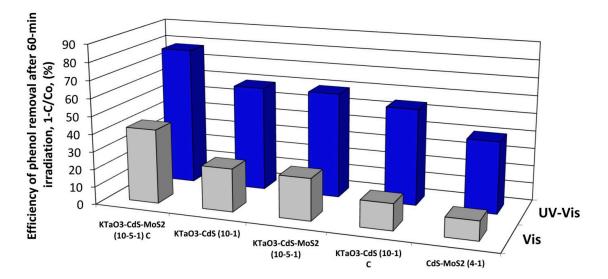


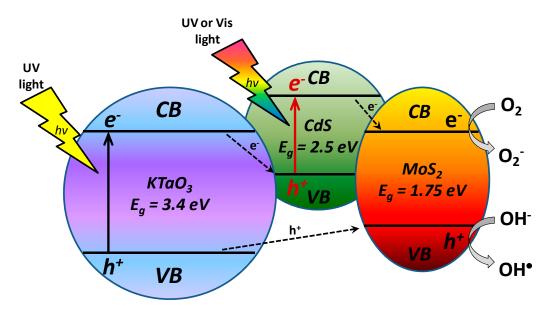**Figure 10.** Probable UV-Vis two-photon excitation cycle of KTaO₃-CdS-MoS₂ composite: (1) UV induced excitation in solid KTaO₃ ($E_g$ = 3.4 eV) to generate free electrons ($e^-$) and holes ($h^+$), and since the VB position of KTaO₃ is lower than the VB band of MoS₂, $h^+$ transfer would then occur from KTaO₃ to MoS₂; (2) UV or visible light excitation of solid CdS ($E_g$ = 2.5 eV) also generates $e^-$ and $h^+$ in CdS, and as the CB position of CdS is higher in energy than the CB of solid MoS₂, electron transfer could occur from CdS to MoS₂, thereby causing a charge separation at the CdS-MoS₂ junction; (3) positioning the CB of KTaO₃ higher in energy than the VB of CdS causes $e^-$ transfer from KTaO₃ to CdS and recombination of $e^-$ in KTaO₃ with $h^+$ generated in CdS, thus completing the photoexcitation cycle in which the excited state of MoS₂ has been achieved via a two-photon process.

## 3. Experimental

### 3.1. Materials and Instruments

Tantalum (V) oxide (>99% Aldrich, Poznan, Poland) and potassium hydroxide (Chempur, pure p.a.) were used as precursors for the preparation of $KTaO_3$. Thiourea (Aldrich, 99%) has been chosen as a sulfur source to synthesize sulfides. $CdCl_2 \cdot 2H_2O$ (Sigma-Aldrich, ≥99%) and $Na_2MoO_4 \cdot 2H_2O$ (Sigma-Aldrich, ≥99.5%) were used as precursors of Cd and Mo, respectively. Ethanol, polyethylene glycol 400 (PEG-400), ethylene glycol (EG) were purchased from POCH S.A. (Gliwice, Poland) and used without further purification. Deionized water was used for all reactions and treatment processes. A commercial form of $TiO_2$ (P25, crystalline composition: 80% anatase, 20% rutile, surface area 50 g/m$^2$) from Evonik (Essen, Germany) was used for the comparison of the photocatalytic activity.

Nitrogen adsorption–desorption isotherms at 77 K were measured using a Micromeritics Gemini V (model 2365) physisorption analyzer (Micromeritics Instrument, Norcross, GA, USA). Specific surface areas were calculated following typical Brunauer–Emmett–Teller (BET) method using the adsorption data in the relative pressure (p/p$_0$) range from 0.05 to 0.3. Prior to adsorption measurements the samples were degassed under vacuum at 200 °C for 2 h.

Diffuse reflectance spectra (DRS) of the synthesized materials were characterized using the Thermo Scientific Evolution 220 UV-Visible spectrophotometer (Thermo Scientific, Waltham, MA, USA) equipped with ISA-220 integrating sphere accessory. The UV-Vis DRS spectra were recorded in the range of 200–800 nm using a barium sulfate reference.

Powder X-ray diffraction (PXRD, Philips/PANalytical X'Pert Pro MPD diffractometer, (PANalytical, Almelo, The Netherlands) with Cu K$_\alpha$ radiation λ = 1.5418 Å) was used to determine the phase composition and calculate lattice parameters of polycrystalline samples.

The morphology of the semiconductor composites was investigated with FEI Quanta 250 FEG scanning electron microscope (SEM; FEI, Hillsboro, OR, USA) working in high vacuum mode. Energy-dispersive X-ray spectroscopy (EDS) measurements were carried out using SEM-integrated EDAX Apollo-SDD detector (EDAX Inc., Mahwah, NJ, USA). Accelerating voltage was set to 30 kV. Standardless analysis was conducted with the EDAX TEAM software with *eZAF* quantization method.

### 3.2. Synthesis of Single KTaO₃, CdS and MoS₂ Semiconductors

$KTaO_3$, CdS and $MoS_2$ semiconductors were prepared by hydro/solvothermal methods using an autoclave with a capacity of 500 mL as the reactor. In a typical procedure for the preparation of potassium tantalate, KOH (30 g) was dissolved in deionized water (60 mL), then $Ta_2O_5$ (11 g) and PEG-400 (3 mL) were added. This mixture (marked as *solution A*) was stirred for 1 h before it was transferred into a Teflon-lined stainless steel autoclave. The autoclave was sealed and got heated at 200 °C for 24 h. After cooling naturally to room temperature, the resulting powder was washed several times by centrifugation with distilled water and ethanol respectively and dried in an oven at 70 °C for 8 h. Finally, some white powder was obtained.

Cadmium sulfide was prepared based on the methodology presented by Zhong *et al.* [42]. In a typical procedure, $CdCl_2$ (18.3 g) was added into deionized water (160 mL) and EG (160 mL) under continuous stirring for 15 min. After that, thiourea (15.2 g) was added to the solution and stirring was

continued for an additional 20 min. This mixture (marked as *solution B*) was transferred into the autoclave which was sealed and maintained at 190 °C for 24 h and allowed to cool down to room temperature naturally. The crystalline powder product was washed several times by centrifugation with distilled water and ethanol, respectively and dried in the oven at 70 °C for 8 h. Finally, some yellow powder was obtained.

Molybdenum disulfide was synthesized using a method similar to reported by Wang *et al.* [46]. To prepare $MoS_2$, $Na_2MoO_4 \cdot 2H_2O$ (12.1 g), thiourea (15.6 g) and PEG-400 (3.5 g) were dissolved in deionized water (300 mL). The solution was stirred continuously for 15 min. The resulting mixture (marked as *solution C*) was transferred into the teflon-lined stainless autoclave which was maintained at 200 °C for 24 h, then cooled to room temperature. The precipitate was washed with deionized water and dried in the oven at 80 °C for 6 h. Finally, some black powder was obtained.

### 3.3. Synthesis of Binary and Ternary Semiconductor Composites

The $KTaO_3$, CdS and $MoS_2$ powders or solutions A, B, C prepared according to the methods described in Section 2.2 were combined to form semiconductor nanocomposites by the calcination or by the hydro/solvothermal mixed solutions methods, respectively. All prepared samples with different molar ratios between semiconductors are presented in Table 1.

To prepare $KTaO_3$-CdS, $KTaO_3$-$MoS_2$ and $KTaO_3$-CdS-$MoS_2$ composites by the calcination method, $KTaO_3$ and CdS or/and $MoS_2$ powders, respectively were mixed together sufficiently with various molar ratios. The powder mixture was calcined in the oven at 500 °C for 3 h with a heating rate of 3 °C/min. Then the heated mixture was removed from the oven and allowed to cool to room temperature naturally.

A typical hydro/solvothermal mixed solutions process for the preparation of CdS-$MoS_2$; $KTaO_3$-CdS; $KTaO_3$-$MoS_2$; $KTaO_3$-CdS-$MoS_2$ composites with various molar ratios between semiconductors was as follows: the required amounts of solutions B and C; A and B; A and C; A and B and C, respectively were mixed together and stirred continuously for 45 min using a magnetic stirrer. Then the as-prepared mixture was placed in the autoclave and heated at 200 °C for 24 h. The resulting precipitate was washed with distilled water and ethanol, respectively and dried in the oven at 70 °C for 8 h.

### 3.4. Measurement of Photocatalytic Activity in the Aqueous Phase

The photocatalytic activity of $KTaO_3$, CdS and $MoS_2$ single semiconductors and their nanocomposite powder in ultraviolet (UV) and visible light (Vis) was estimated by monitoring the decomposition rate of 0.21 mM phenol in the aqueous solution. Phenol was selected as a model contaminant because it is a non-volatile and common organic pollutant found in various types of industrial wastewater. Photocatalytic degradation runs were preceded by blind tests in the absence of a photocatalyst or illumination. The aqueous phase containing the photocatalyst (125 mg), deionized water (24 mL) and phenol (1 mL, C = 500 mg/dm$^3$) was placed in a photocatalytic reactor (V = 25 cm$^3$) equipped with a 30 mm-thick quartz window. The temperature of the aqueous phase during the experiments was maintained at 10 °C by an external circulating water bath. The prepared suspension was stirred using magnetic stirrer and aerated (V = 5 dm$^3$/h) for 30 min in the dark to reach the adsorption equilibrium and then the content of the reactor was photoirradiated with a 1000 W Xenon lamp (Oriel Instruments,

Stratford, CT, USA) which emitted both UV and Vis irradiation. The optical path included a water filter and glass filters (GG420, Optel, Opole, Poland) to cut off IR and/or UV, respectively. GG glass filter transmitted light of wavelength greater than 420 nm. During the irradiation, 1 cm$^3$ of suspension sample was collected at regular time periods and filtered through syringe filters (Ø = 0.2 μm) to remove the photocatalyst particles. Phenol concentration was estimated by colorimetric method after derivatization with diazo-*p*-nitroaniline using UV-Vis spectrophotometer (DU-7, Beckman, Warsaw, Poland).

*3.5. Measurement of Photocatalytic Activity in the Gas Phase*

The photocatalytic activity of the prepared semiconductors and their nanocomposite powders was also determined in the toluene degradation process. Toluene, an important volatile organic compound (VOC), was used as a model air contaminant. The photocatalysts activity tests were carried out in the flat stainless steel reactor (V = 30 cm$^3$) equipped with a quartz window, two valves and a septa. As an irradiation source there was used an array of 25 LEDs ($\lambda_{max}$ = 375 nm, 63 mW per diode) which was described in our previous study [47]. In a typical measurement the semiconductor powder (about 0.1 g) was suspended in a small amount of water and loaded as a thick film on a glass plate (3 cm × 3 cm) using painting technique. The obtained semiconductors coated support was dried and then placed at the bottom side of the photoreactor followed by closing the reactor with a quartz window. The gaseous mixture from a cylinder was passed through the reactor space for 1 min. The concentration of toluene in a gas mixture was about 150 ppm. After closing the valves, the reactor was kept in the dark for 15 min to reach adsorption equilibrium. A reference sample was taken just before starting irradiation. To estimate toluene concentration the samples were taken every 10 min during 60 min of irradiation. The photocatalytic stability was estimated in four subsequent cycles of toluene degradation. The analysis of toluene concentration in the gas phase was carried out using a Perkin Elmer Clarus 500 GC (Perkin Elmer, Waltham, MA, USA) equipped with a 30 m × 0.25 mm Elite-5 MS capillary column (0.25 μm film thickness) and a flame ionization detector (FID). The samples (200 μL) were injected by using a gas-tight syringe. Helium was used as a carrier gas at a flow rate of 1 mL/min.

**4. Conclusions**

A series of novel binary and ternary composite photocatalysts was obtained based on the combination of potassium tantalate, cadmium sulfide and molybdenum disulfide powders as well as their hydro/solvothermal precursor solutions. It was observed that calcination is an effective method to prepare various KTaO$_3$, CdS and MoS$_2$ semiconductor combinations, the while solvothermal mixed precursor solutions route led to obtaining other composite components. The UV-Vis DRS spectra showed that the loading MoS$_2$ onto CdS shifted absorbance peaks to longer wavelengths as well as loading CdS onto KTaO$_3$ enhanced absorption properties. On the other hand, an excess of MoS$_2$ in composite caused a decrease in activity both for phenol and toluene degradation. It may be suggested that the best absorption properties and the highest activity could probably be achieved for the ternary composites containing appropriate molar ratio between above semiconductors but it needs further investigation. We found that the ternary semiconductor hybrid prepared by calcination of KTaO$_3$, CdS and MoS$_2$ powders at the 10:5:1 molar ratio exhibited very good stability during four measurement cycles in toluene degradation and excellent photocatalytic performance in phenol degradation among

all obtained photocatalysts–the activity reached 80% under UV-Vis and 42% under Vis light 60-min irradiation. This relatively high photoactivity under visible light could be related to the presence of heterojunction between semiconductors. Due to the band structure of component semiconductors, two-photon excitation together with charge carrier transfer between $KTaO_3$, CdS and $MoS_2$ could be expected. However, ternary composite with 10:1:1 molar ratio between semiconductors exhibited relatively low activity which proved that the photocatalytic efficiency in aqueous phase reaction strictly depends on amount of composite components and need further investigation. In general, this work demonstrates that novel composites based on $KTaO_3$, CdS and $MoS_2$ are promising as photocatalysts for the degradation of organic pollutants in both the gas and aqueous phases.

## Acknowledgments

## Author Contributions

AZ designed research; BB, AC, MJW, TK and AZ performed research and analyzed the data; BB, AC, TK and AZ wrote the paper. All authors read and approved the final manuscript.

## Conflicts of Interest

The authors declare no conflict of interest.

## References

1. Fujishima, A.; Honda, K. Electrochemical photolysis of water at a semiconductor electrode. *Nature* **1972**, *238*, 37–38.
2. Chen, X.B.; Mao, S.S. Titanium dioxide nanomaterials: Synthesis, properties, modifications, and applications. *Chem. Rev.* **2007**, *107*, 2891–2959.
3. Tong, H.; Ouyang, S.X.; Bi, Y.P.; Umezawa, N.; Oshikiri, M.; Ye, J.H. Nanophotocatalytic materials: Possibilities and challenges. *Adv. Mater.* **2012**, *24*, 229–251.
4. Bahnemann, D. Photocatalytic water treatment: Solar energy applications. *Sol. Energy* **2004**, *77*, 445–459.
5. Ahmad, M.; Ahmed, E.; Zhang, Y.W.; Khalid, N.R.; Xu, J.F.; Ullah, M.; Hong, Z.L. Preparation of highly efficient *Al*-doped ZnO photocatalyst by combustion synthesis. *Curr. Appl. Phys.* **2013**, *4*, 697–704.
6. Liao, C.H.; Huang, C.W.; Wu, J.C.S. Hydrogen production from semiconductor-based photocatalysis via water splitting. *Catalysts* **2012**, *2*, 490–516.
7. Zhang, N.; Ciriminna, R.; Pagliaro, M.; Xu, Y.-J. Nanochemistry-derived $Bi_2WO_6$ nanostructures: Towards production of sustainable chemicals and fuels induced by visible light. *Chem. Soc. Rev.* **2014**, *43*, 5276–5287.

8. Zhang, N.; Zhang, Y.; Xu, Y.-J. Recent progress on graphene-based photocatalysts: Current status and future perspectives. *Nanoscale* **2012**, *4*, 5792–5813.

9. Zhang, N.; Liu, S.; Xu, Y.-J. Recent progress on metal core@semiconductor shell nanocomposites as a promising type of photocatalyst. *Nanoscale* **2012**, *4*, 2227–2238.

10. Pan, X.; Yang, M.-Q.; Fu, X.; Zhang, N.; Xu, Y.-J. Defective $TiO_2$ with oxygen vacancies: Synthesis, properties and photocatalytic applications. *Nanoscale* **2013**, *5*, 3601–3614.

11. Yang, M.-Q.; Xu, Y.-J. Selective photoredox using graphene-based composite photocatalysts. *Phys. Chem. Chem. Phys.* **2013**, *15*, 19102–19118.

12. Fujishima, A.; Zhang, X.; Tryk, D.A. $TiO_2$ photocatalysis and related surface phenomena. *Surf. Sci. Rep.* **2008**, *63*, 515–582.

13. Marschall, R. Semiconductor composites: Strategies for enhancing charge carrier separation to improve photocatalytic activity. *Adv. Funct. Mater.* **2014**, *17*, 2420–2440.

14. Yang, G.; Yan, Z.; Xiao, T. Preparation and characterization of $SnO/ZnO/TiO_2$ composite semiconductor with enhanced photocatalytic activity. *Appl. Surf. Sci.* **2012**, *258*, 8704–8712.

15. Emeline, A.V.; Kuznetsov, V.N.; Ryabchuk, V.K.; Serpone, N. On the way to the creation of next generation photoactive materials. *Environ. Sci. Pollut. Res.* **2012**, *19*, 3666–3675.

16. Serpone, N.; Emeline, A.V. Semiconductor photocatalysis—Past, present, and future outlook. *J. Phys. Chem. Lett.* **2012**, *3*, 673–677.

17. Zhang, Y.; Tang, Z.-R.; Fu, H.; Xu, Y.-J. $TiO_2$-graphene nanocomposites for gas-phase photocatalytic degradation of volatile aromatic pollutant: Is $TiO_2$-graphene truly different from other $TiO_2$-carbon composite materials? *ACS Nano* **2010**, *4*, 7303–7314.

18. Kato, H.; Kudo, A. Photocatalytic water splitting into $H_2$ and $O_2$ over various tantalate photocatalysts. *Catal. Today* **2003**, *78*, 561–569.

19. Liu, J.W.; Chen, G.; Li, Z.H.; Zhang, Z.G. Hydrothermal synthesis and photocatalytic properties of $ATaO_3$ and $AnbO_3$ (A = Na and K). *Int. J. Hydrogen Energy* **2007**, *32*, 2269–2272.

20. Kudo, A. Development of photocatalyst materials for water splitting. *Int. J. Hydrog. Energy* **2006**, *31*, 197–202.

21. Lin, W.; Chen, C.; Hu, C.; Teng, H. $NaTaO_3$ photocatalysts of different crystalline structures for water splitting into $H_2$ and $O_2$. *Appl. Phys. Lett.* **2006**, *89*, 211904.

22. Torres-Martínez, L.M.; Cruz-López, A.; Juárez-Ramírez, I.; Meza-de la Rosa, M.E. Methylene blue degradation by $NaTaO_3$ sol-gel doped with Sm and La. *J. Hazard. Mater.* **2009**, *165*, 774–779.

23. Zhu, H.; Jiang, R.; Xiao, L.; Chang, Y.; Guan, Y.; Li, X.; Zeng, G. Photocatalytic decolorization and degradation of Congo Red on innovative crosslinked chitosan/nano-CdS composite catalyst under visible light irradiation. *J. Hazard. Mater.* **2009**, *169*, 933–940.

24. Zhai, T.Y.; Fang, X.S.; Bando, Y.S.; Liao, Q.; Xu, X.J.; Zeng, H.B.; Ma, Y.; Yao, J.N.; Golberg, D. Morphology-dependent stimulated emission and field emission of ordered CdS nanostructure arrays, *ACS Nano* **2009**, *3*, 949–959.

25. Dongre, J.K.; Nogriya, V.; Ramrakhiani, M. Structural, optical and photoelectrochemical characterization of CdS nanowire synthesized by chemical bath deposition and wet chemical etching. *Appl. Surf. Sci.* **2009**, *255*, 6115–6120.

26. Zhang, H.; Zhu, Y. Significant visible photoactivity and antiphotocorrosion performance of CdS photocatalysts after monolayer polyaniline hybridization. *J. Phys. Chem. C* **2010**, *114*, 5822–5826.

27. Zhong, M.; Shi, J.; Xiong, F.; Zhang, W.; Li, C. Enhancement of photoelectrochemical activity of nanocrystalline CdS photoanode by surface modification with $TiO_2$ for hydrogen production and electricity generation. *Sol. Energy* **2012**, *86*, 756–763.

28. Li, X.; Xia, T.; Xu, C.; Murowchick, J.; Chen, X. Synthesis and photoactivity of nanostructured CdS–$TiO_2$ composite catalysts. *Catal. Today* **2014**, *225*, 64–73.

29. He, D.; Chen, M.; Teng, F.; Li, G.; Shi, H.; Wang, J.; Xu, M.; Lu, T.; Ji, X.; Lv, Y. Enhanced cyclability of CdS/$TiO_2$ photocatalyst by stable interface structure. *Superlattices Microstruct.* **2012**, *51*, 799–808.

30. Panigrahi, S.; Basak, D. Morphology driven ultraviolet photosensitivity in ZnO–CdS composite. *J. Colloid Interface Sci.* **2011**, *364*, 10–17.

31. Jana, T.K.; Pal, A.; Chatterjee, K. Self assembled flower like CdS–ZnO nanocomposite and its photo catalytic activity. *J. Alloys Compd.* **2014**, *583*, 510–515.

32. Liu, S.; Li, H.; Yan, L. Synthesis and photocatalytic activity of three-dimensional ZnS/CdS composites. *Mater. Res. Bull.* **2013**, *48*, 3328–3334.

33. Liu, X.; Yan, Y.; Da, Z.; Shi, W.; Ma, C.; Lv, P.; Tang, Y.; Yao, G.; Wu, Y.; Huo, P.; *et al.* Significantly enhanced photocatalytic performance of CdS coupled $WO_3$ nanosheets and the mechanism study. *Chem. Eng. J.* **2014**, *241*, 243–250.

34. Zhao, Y.; Zhang, Y.; Yang, Z.; Yan, Y.; Sun, K. Synthesis of $MoS_2$ and $MoO_2$ for their applications in $H_2$ generation and lithium ion batteries: A review. *Sci. Technol. Adv. Mater.* **2013**, *14*, 043501.

35. Zong, X.; Wu, G.; Yan, H.; Ma, G.; Shi, J.; Wen, F.; Wang, L.; Li, C. Photocatalytic $H_2$ Evolution on $MoS_2$/CdS Catalysts under Visible Light Irradiation. *J. Phys. Chem. C* **2010**, *114*, 1963–1968.

36. Chen, G.; Li, D.; Li, F.; Fan, Y.; Zhao, H.; Luo, Y.; Yu, R.; Meng, O. Ball-milling combined calcination synthesis of $MoS_2$/CdS photocatalysts for high photocatalytic $H_2$ evolution activity under visible light irradiation. *Appl. Cat. A* **2012**, *443–444*, 138–144.

37. Liu, Y.; Yu, Y.X.; Zhang, W.D. $MoS_2$/CdS Heterojunction with high photoelectrochemical activity for $H_2$ evolution under visible light: The Role of $MoS_2$. *J. Phys. Chem. C* **2013**, *117*, 12949–12957.

38. Liu, Y.; Yu, H.; Quan, X.; Chen, S. Green synthesis of feather-shaped $MoS_2$/CdS photocatalyst for effective hydrogen production. *Int. J. Photoenergy* **2013**, *2013*, 247516–247520.

39. Zong, X.; Yan, H.; Wu, G.; Ma, G.; Wen, F.; Wang, L.; Li, C. Enhancement of photocatalytic $H_2$ evolution on CdS by loading $MoS_2$ as cocatalyst under visible light irradiation. *J. Am. Chem. Soc.* **2008**, *130*, 7176–7177.

40. Wiedemeier, H.; Khan, A.A. Phase studies in the system managanese sulfioe–cadmium sulfide. *Trans. Metall. Soc. AIME* **1968**, *242*, 1969–1972.

41. Hu, C.-C.; Yeh, T.-F.; Teng, H. Pyrochlore-like $K_2Ta_2O_8$ synthesized from different methods as efficient photocatalysts for water splitting. *Catal. Sci. Technol.* **2013**, *3*, 1798–1804.

42. Zhong, S.; Zhang, L.; Huang, Z.; Wang, S. Mixed-solvothermal synthesis of CdS micro/nanostructures and their optical properties. *Appl. Surf. Sci.* **2011**, *257*, 2599–2603.

43. Zou, Y.; Hu, Y.; Gu, H.; Wang, Y. Optical properties of octahedral $KTaO_3$ nanocrystalline. *Mater. Chem. Phys.* **2009**, *115*, 151–153.

44. Adhikari, R.; Malla, S.; Gyawali, G.; Sekino, T.; Lee, S.W. Synthesis, characterization and evaluation of the photocatalytic performance of Ag-$CdMoO_4$ solar light driven plasmonic photocatalysts. *Mat. Res. Bull.* **2013**, *48*, 3367–3373.

45.  Wang, W.-S.; Zhen, L.; Xu, C.-Y.; Shao, W.-Z.; Chen, Z.-L. Formation of CdMO$_4$ porous hollow nanospheres via self-assembly accompanied with Ostwald ripening process and their photocatalytic performance. *CrystEngComm* **2013**, *15*, 8014–8021.
46.  Wang, S.; Li, G.; Du, G.; Jiang, X.; Feng, C.; Guo, Z.; Kim, S. Hydrothermal synthesis of molybdenum disulfide for lithium ion battery applications. *Chin. J. Chem. Eng.* **2010**, *18*, 910–913.
47.  Nischk, M.; Mazierski, P.; Gazda, M.; Zaleska, A. Ordered TiO$_2$ nanotubes: The effect of preparation parameters on the photocatalytic activity in air purification process. *Appl. Catal. B* **2014**, *144*, 674–685.

*Sample Availability*: Samples of the compounds are available from the authors.